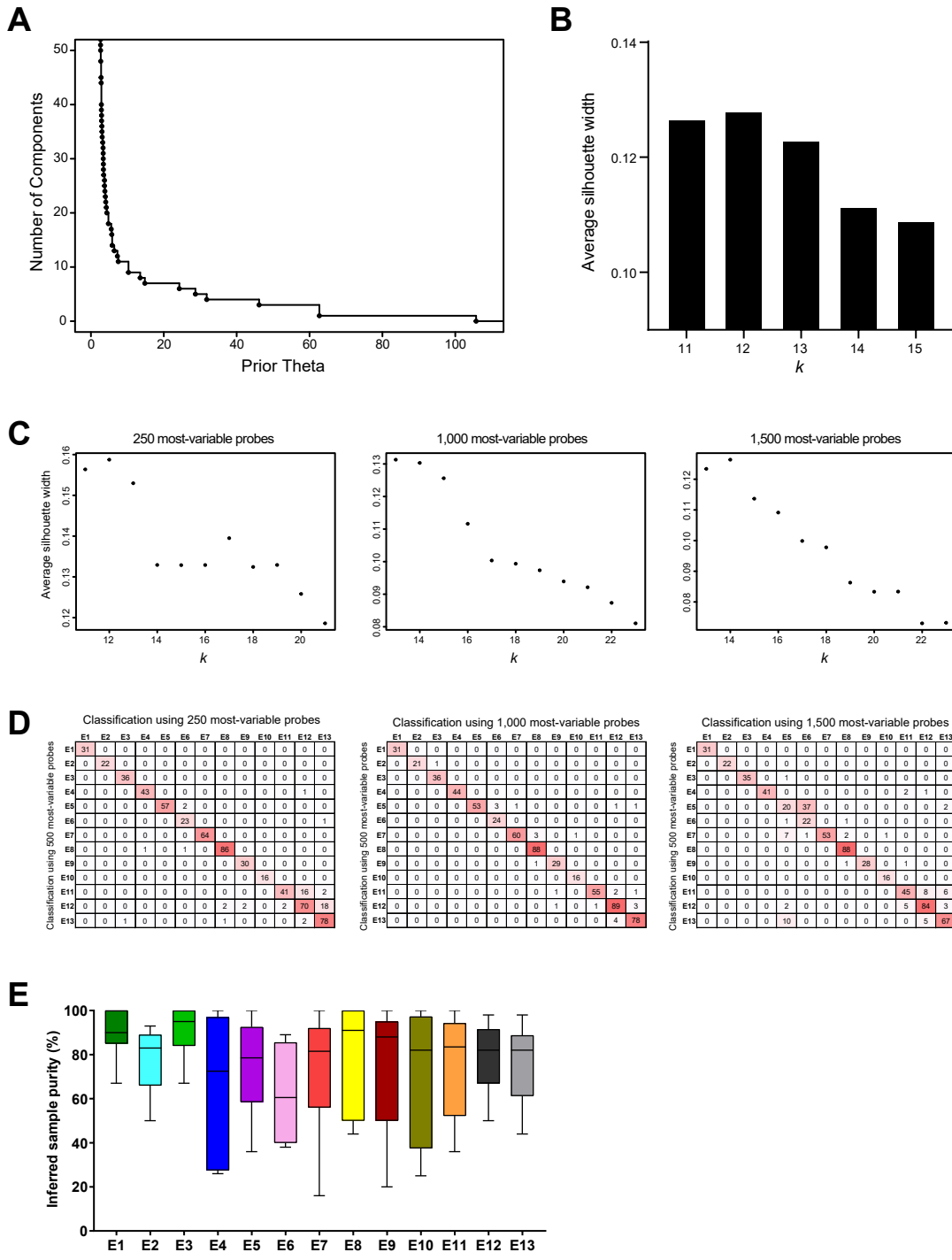
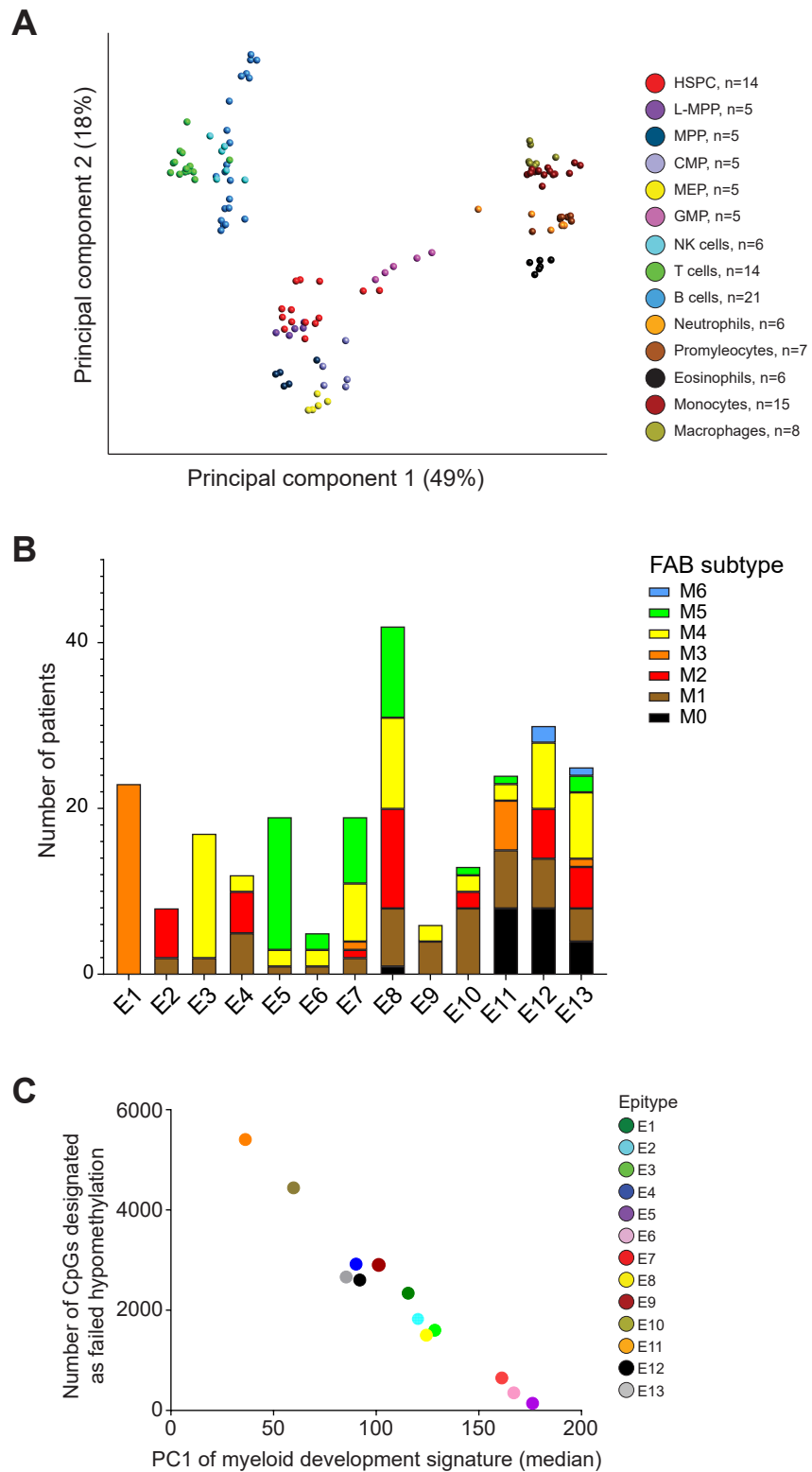


Supplemental Figure S1:



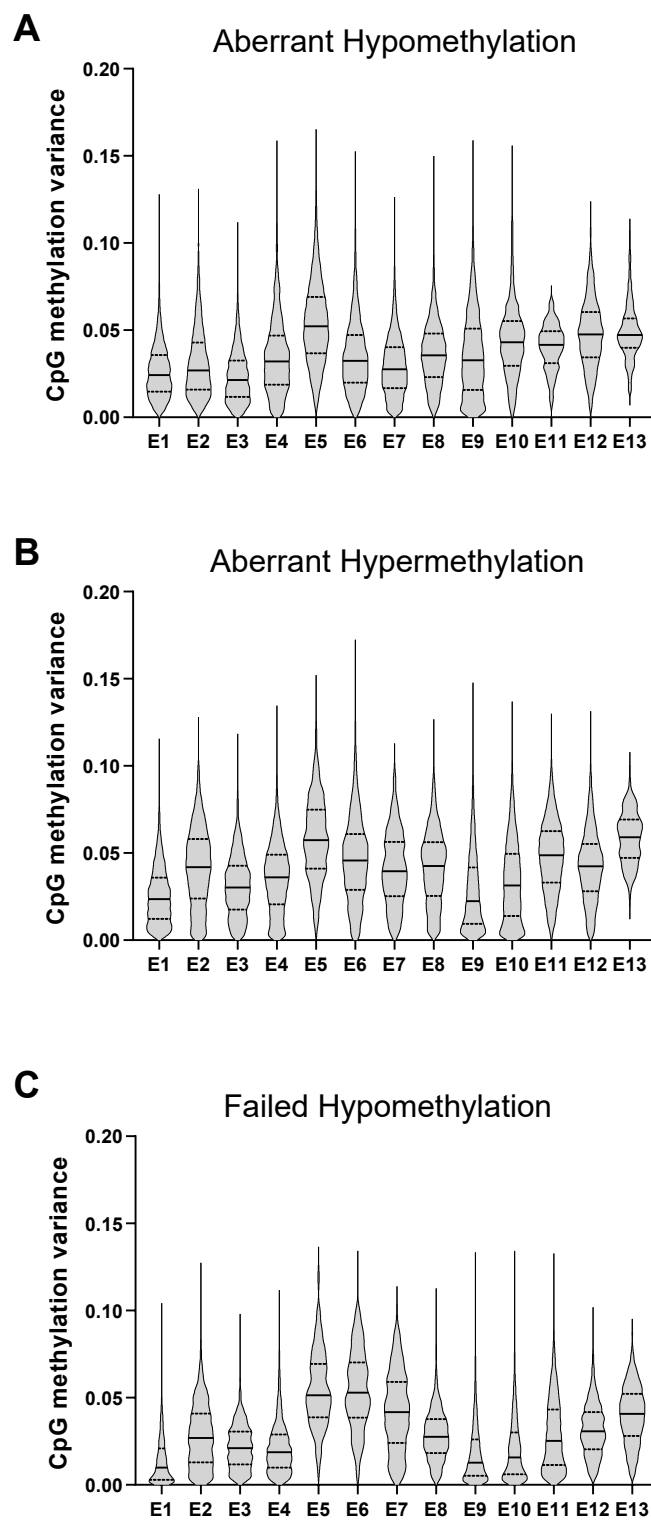
Supplemental Figure S1: Evaluation of unsupervised clustering. (A) The Auer Gervini method employing a Bayesian sensitivity analysis was used to plot a step function displaying the prior theta as the number of principal components increases. A large step length is defined by the first step that is twice the mean step length. (B) Average silhouette width following PAM clustering with increasing k starting at 11 subgroups. (C) Average silhouette when varying the total number of most-variable probes used from 500 to 250, 1,000 and 1,500. (D) Classification tables identifying how varying the number of probes impacts the classification of samples into epitypes after changing the number of most-variable probes from 500 to 250, 1,000 and 1,500. The total number of differentially-classified samples were 49/649 (7.6%) for 250 probes, 25/649 (3.9%) for 1,000 probes, and 79/649 (12.2%) for 1,500 probes. The samples that displayed a different classification were mainly observed between E5 versus E6, and within the stem-supercluster (E11-13). (E) Tumor cell purity across epitypes in the TCGA cohort assessed using the ABSOLUTE algorithm.

Supplemental Figure S2:



Supplemental Figure S2: AML epitypes occupy discrete stages of development between HSPCs and monocytes. (A) Principal component analysis of the most-variable CpGs between 14 normal hematopoietic subpopulations showing branching of lymphoid and myeloid cell types. This set of 28,360 CpGs defines the hematologic developmental probe set used in Fig. 2A. (B) The distribution of FAB classifications within each epitype. (C) Correlation between the number of hypomethylated probes and the 1st principal component from PCA analysis displayed in Fig. 2B.

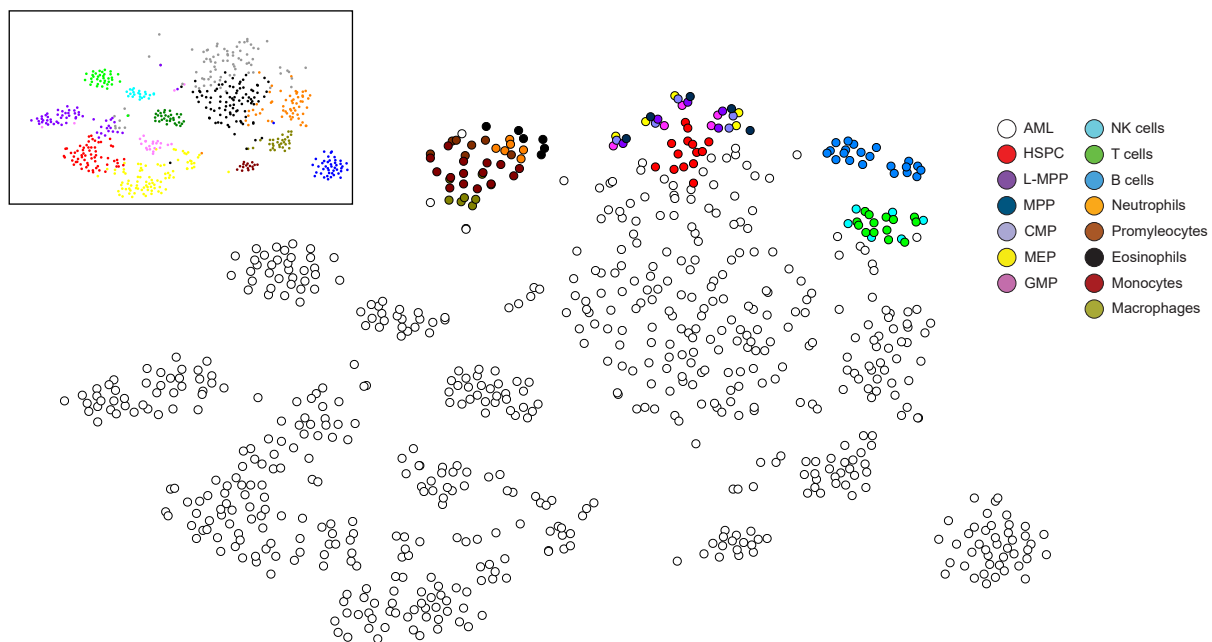
Supplemental Figure S3:



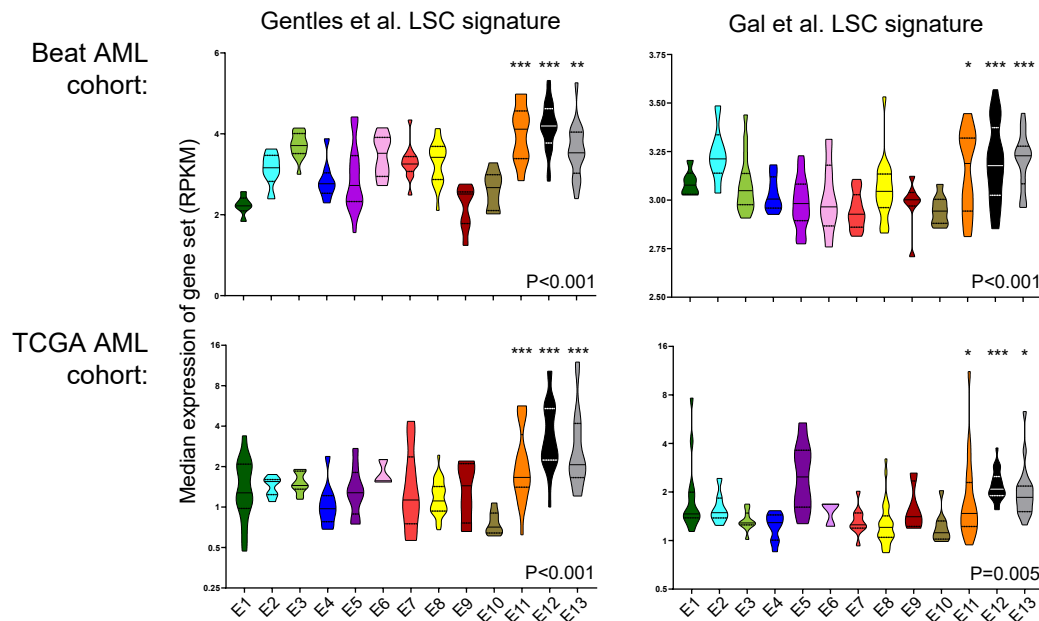
Supplemental Figure S3: Variance among CpG methylation values for all CpGs that are classified as differentially methylated, including (A) aberrant hypermethylation, (B) aberrant hypomethylation, and (C) failed hypomethylation within individual epitypes. The numbers of CpGs for each differentially methylation category per epitype are shown in Figure 2E.

Supplemental Figure S4:

A

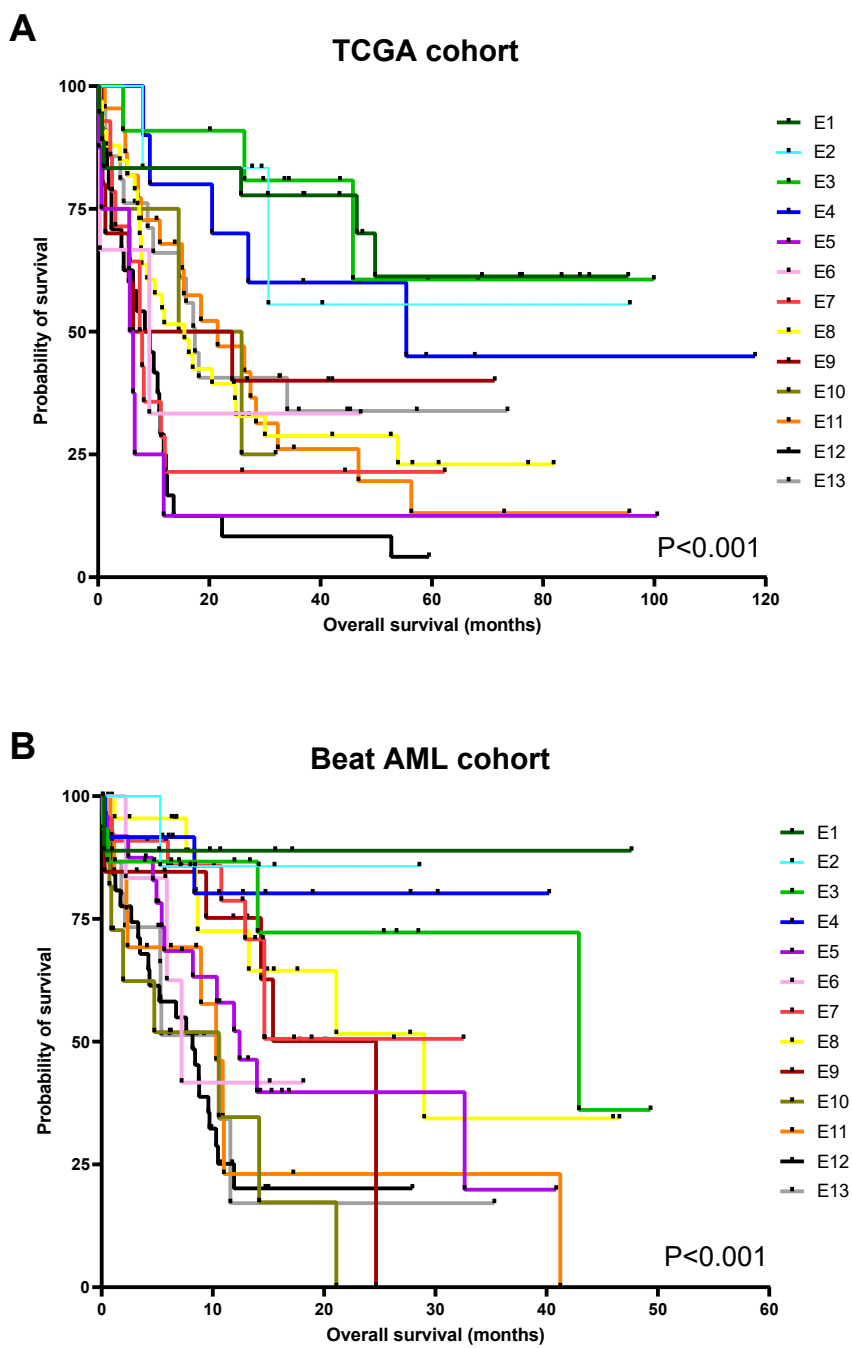


B



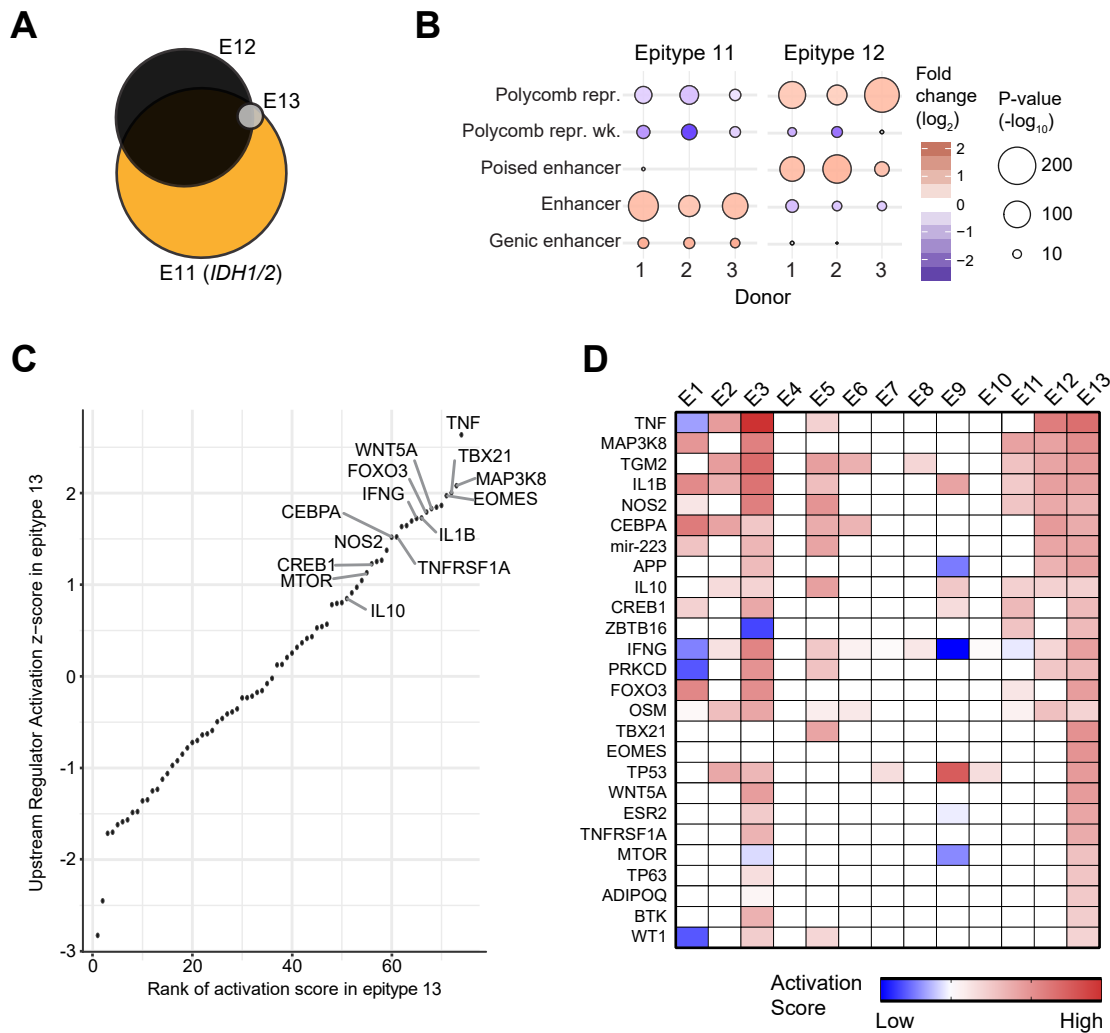
Supplemental Figure S4: The relationship between epitypes E11-E13 and hematopoietic stem cells using epigenetic and gene expression signatures. (A) tSNE plot of the epityping probe set used in Figure 1 showing AML samples (white) combined with normal cell types including stem and progenitor populations (colored). Inset shows the same tSNE plot with standard colors for AML epitypes for reference. (B) Median expression value of genes within hematopoietic stem cell gene sets from Gal et al. and Gentiles et al. AML samples were separated by epitype and assessed separately in the Beat AML cohort (top panels) and the TCGA cohort (bottom panels). Overall significance tested by ANOVA, followed by comparison of E11-13 individually versus E1-10; adjusted p-values *P<0.05, **P<0.01, ***P<0.001.

Supplemental Figure S5:



Supplemental Figure S5: Kaplan-Meier plots showing the overall survival of patients separated by epitype in (A) TCGA and (B) Beat AML cohorts.

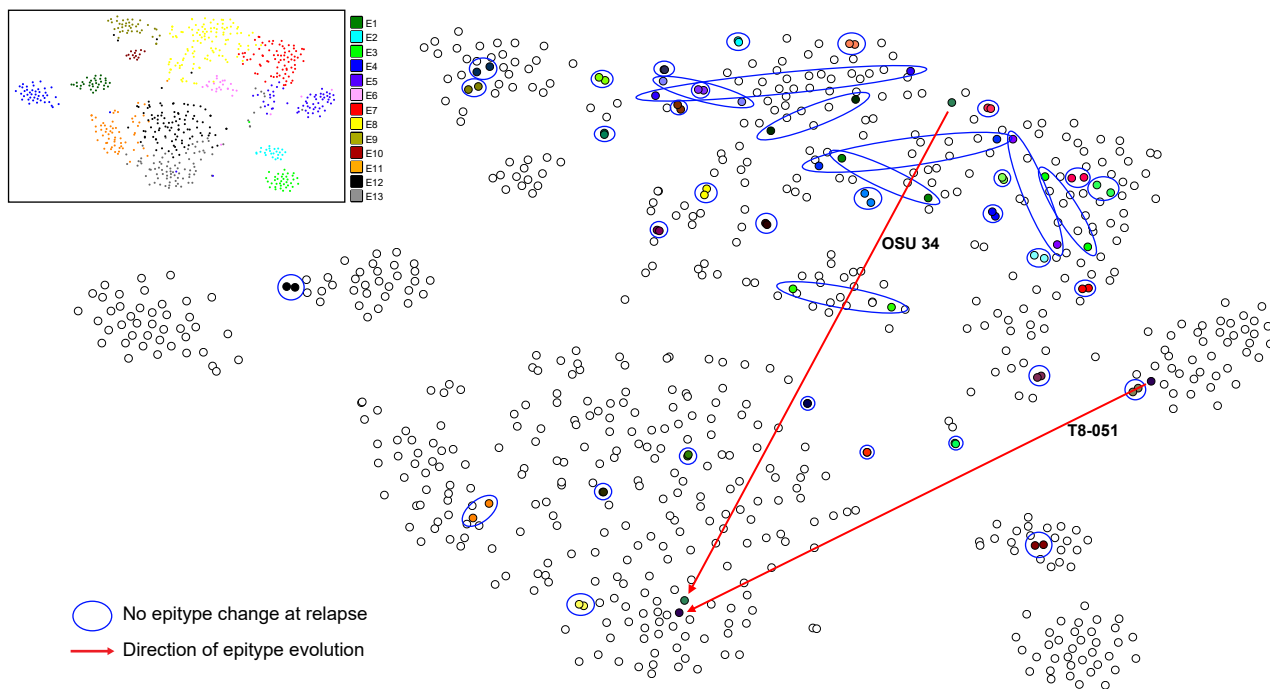
Supplemental Figure S6:



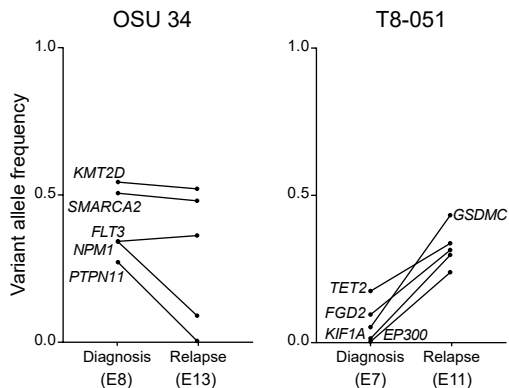
Supplemental Figure S6: AML epitypes E11-E13 display elevated inflammatory signaling. (A) Venn diagram of aberrant hypermethylation in epitypes E11-E13. (B) Enrichment of aberrantly hypermethylated regions in chromatin states in 3 independent HSPC samples. Chromatin states involving polycomb repression and enhancers are shown (repr., repressed). (C) Plot of IPA upstream regulator activation score in epitype E13. Pathways were ranked by activation score and those relevant to myelopoiesis and involved in inflammatory signaling are highlighted. (D) Heatmap displaying the upstream regulator activation score using IPA across all epitypes sorted by activation score in E11-13.

Supplemental Figure S7:

A



B



Supplemental Figure S7: Validation of infrequent epitype evolution at relapse. (A) tSNE plot of the AML epityping probe set including all AML samples along with 41 paired diagnosis/relapse samples from the validation cohort. Diagnosis/relapse pairs are indicated by the same color, pairs not changing epitype are circled in blue. Red arrows indicate pairs where the relapse sample changed epitype. Distribution of epitypes are illustrated in the framed tSNE plot (inset). (B) Variant allele frequency of mutations between diagnosis and relapse in the 2/41 pairs that changed epigenetic epitype. To ensure sufficiently equal purity at diagnosis and relapse, patients were excluded from the study that did not have a tumor-specific mutation >0.3 VAF at both diagnosis and relapse. Tumor mutation specificity was determined by the absence of the mutation at remission. The absence of tumor-specific mutations were also required to indicate clearance of tumor cells following treatment.

Supplementary Table 7: Multivariate analyses of the LSC17 (high versus low) and the stem-like supercluster (E11-E13) versus other epitypes (E1-E10).

Beat AML cohort

LSC17 high vs LSC17 low

n=168

Variable	Categories	P-value	Hazard Ratio (95% CI)
LSC17	High vs Low	0.009	1.65 (1.13, 2.41)

Stem cluster: Stem-like vs other

n=168

Variable	Categories	P-value	Hazard Ratio (95% CI)
E11-E13	E11-E13 vs E1-E10	0.03	1.53 (1.05, 2.22)

Both

n=168

Variable	Categories	P-value	Hazard Ratio (95% CI)
LSC17	High vs Low	0.06	1.49 (0.98, 2.27)
E11-E13	E11-E13 vs E1-E10	0.27	1.27 (0.834, 1.94)

TCGA cohort

LSC17 high vs LSC17 low

n=139

Variable	Categories	P-value	Hazard Ratio (95% CI)
LSC17	High vs Low	0.13	1.46 (0.90, 2.39)

Stem cluster: Stem-like vs other

n=139

Variable	Categories	P-value	Hazard Ratio (95% CI)
E11-E13	E11-E13 vs E1-E10	<0.001	3.12 (1.92, 5.06)

Both

n=139

Variable	Categories	P-value	Hazard Ratio (95% CI)
LSC17	High vs Low	0.43	1.22 (0.74, 2.02)
E11-E13	E11-E13 vs E1-E10	<0.001	3.02 (1.84, 4.94)